29^{th} Symposium on Naval Hydrodynamics
Gothenburg, Sweden, 26-31 August 2012

Towards LES of High Reynolds Number External Flows on Unstructured Grids

Aman Verma and Krishnan Mahesh
(University of Minnesota, USA)

ABSTRACT

Large eddy simulation (LES) using the dynamic Smagorinsky model (DSM) (Germano et al., 1991) and discretely kinetic energy conserving numerical methods (Mahesh et al., 2004) has successfully predicted complex flows such as gas turbine combustors and marine propulsor crashback (e.g. Vyšohlid and Mahesh (2005); Chang et al. (2008); Jang and Mahesh (2010, 2012); Verma et al. (2012)). This paper discusses two developments towards reliably using LES for inhomogeneous and attached flows: (1) a dynamic Lagrangian model where a dynamic procedure is proposed for the Lagangian timescale and (2) a wall model where in addition to the Germano-identity error, external Reynolds stress is also imposed as a constraint on the ensemble-average subgrid-scale stress. Both developments are for unstructured grids.

INTRODUCTION

Many practical flows of engineering interest such as flow past a submarine, ship wakes, etc. are high Reynolds number (Re) flows. It has been estimated that the grid requirement for a Direct Numerical Simulation (DNS) scales with the Reynolds number as $Re_\tau^{9/4}$. High Reynolds number flows exhibit such a large range of length and time scales that DNS are rendered impossible for the foreseeable future. Large eddy simulation (LES) is a viable analysis and design tool for complex flows due to advances in massive parallel computers and numerical techniques. LES is essentially an under-resolved turbulence simulation using a model for the subgrid-scale (SGS) stress to account for the inter-scale interaction between the resolved and the unresolved scales. The success of LES relies on the dominance of the large, geometry dependent, resolved scales in determining important flow dynamics and statistics.

In LES, the large scales are directly accounted for by the spatially filtered N-S equations and the small scales are modeled. The spatially filtered incompressible Navier-Stokes equations are

$$\begin{gathered}\frac{\partial \overline{u}_i}{\partial t} + \frac{\partial}{\partial x_j}(\overline{u}_i\overline{u}_j) = -\frac{\partial \overline{p}}{\partial x_i} + \nu\frac{\partial^2 \overline{u}_i}{\partial x_j \partial x_j} - \frac{\partial \tau_{ij}}{\partial x_j} \\ \frac{\partial \overline{u}_i}{\partial x_i} = 0\end{gathered} \tag{1}$$

where x_i denotes the spatial coordinates, u_i is the velocity field, p is the pressure, ν is the kinematic viscosity, $\overline{()}$ denotes the spatial filter at scale Δ and $\tau_{ij} = \overline{u_i u_j} - \overline{u}_i\overline{u}_j$ is the SGS stress.

It is generally assumed that small scales are more universal and isotropic than large scales; eddy viscosity type SGS models are therefore widely used in LES. The original Smagorinsky model (Smagorinsky, 1963) is a simple model for the SGS stress in terms of the local resolved flow

$$\tau_{ij} - \frac{1}{3}\tau_{kk}\delta_{ij} = -2(C_s\Delta)^2|\overline{S}|\overline{S}_{ij} = -2\nu_t\overline{S}_{ij} \tag{2}$$

where C_s is a global, adjustable, model coefficient, Δ is the filter width, $\overline{S}_{ij}$ is the strain rate tensor, $|\overline{S}| = (2\overline{S}_{ij}\overline{S}_{ij})^{1/2}$ and $\nu_t = (C_s\Delta)^2|\overline{S}|$ is the eddy-viscosity.

The Dynamic Smagorinsky model (DSM) (Germano et al., 1991) is a widely used model. It is based on the Germano identity and dynamically computes the model coefficient from the resolved flow and allows it to vary in space and time. The dynamic procedure to obtain the SGS model coefficient C_s attempts to minimize the Germano-identity error (GIE),

$$\begin{aligned}\epsilon_{ij} &= T_{ij}^d - \widehat{\tau}_{ij}^d - L_{ij}^d \\ &= 2(C_s\Delta)^2\left[\widehat{|\overline{S}|\overline{S}_{ij}} - \left(\frac{\widehat{\Delta}}{\Delta}\right)^2|\widehat{\overline{S}}|\widehat{\overline{S}}_{ij}\right] - L_{ij}^d \\ &= (C_s\Delta)^2 M_{ij} - L_{ij}^d,\end{aligned} \tag{3}$$

where $\widehat{()}$ denotes test filtering at scale $\widehat{\Delta}$ and is usually taken to be $\widehat{\Delta} = 2\Delta$, deviatoric parts (denoted by $()^d$) of τ_{ij} and T_{ij} are modeled by using the Smagorinsky model at scales Δ and $\widehat{\Delta}$, $M_{ij} = 2\left[\widehat{|\overline{S}|\overline{S}}_{ij} - \left(\frac{\widehat{\Delta}}{\Delta}\right)^2 |\widehat{\overline{S}}|\widehat{\overline{S}}_{ij}\right]$, and $L_{ij} = \widehat{\overline{u}_i\overline{u}_j} - \widehat{\overline{u}}_i\widehat{\overline{u}}_j$.

Since $\epsilon_{ij}(C_s) = 0$ is a tensor equation, C_s is overdetermined. The original DSM due to Germano et al. (1991) satisfies $\epsilon_{ij}S_{ij} = 0$ to obtain C_s. Lilly (1992) found the equations to be better behaved when minimizing ϵ_{ij} in a least-square sense, yielding

$$(C_s\Delta)^2 = \frac{\langle L_{ij}M_{ij}\rangle}{\langle M_{ij}M_{ij}\rangle} \tag{4}$$

where $\langle\cdot\rangle$ denotes averaging over homogeneous direction(s) and was required to regularize C_s.

However the requirement of averaging over at least one homogeneous direction is impractical for complex inhomogeneous flows. To enable averaging in inhomogeneous flows, Meneveau et al. (1996) developed a Lagrangian version of DSM (LDSM) where C_s is averaged along fluid trajectories. Lagrangian averaging is physically appealing considering the Lagrangian nature of the turbulence energy cascade (Meneveau and Lund, 1994; Choi et al., 2004).

In essence, the Lagrangian DSM attempts to minimize the pathline average of the local GIE squared. The objective function to be minimized is given by

$$\begin{aligned} E &= \int_{pathline} \epsilon_{ij}(\mathbf{z})\epsilon_{ij}(\mathbf{z})d\mathbf{z} \\ &= \int_{-\infty}^{t} \epsilon_{ij}(\mathbf{z}(t'),t')\epsilon_{ij}(\mathbf{z}(t'),t')W(t-t')dt' \end{aligned} \tag{5}$$

where $\mathbf{z}$ is the trajectory of a fluid particle for earlier times $t' < t$ and W is a weighting function to control the relative importance of events near time t, with those at earlier times.

Choosing the time weighting function of the form $W(t-t') = T^{-1}e^{-(t-t')/T}$ yields two transport equations for the Lagrangian average of the tensor products $L_{ij}M_{ij}$ and $M_{ij}M_{ij}$ as $\mathcal{I}_{LM}$ and $\mathcal{I}_{MM}$ respectively:

$$\begin{aligned} \frac{D\mathcal{I}_{LM}}{Dt} &\equiv \frac{\partial\mathcal{I}_{LM}}{\partial t} + \overline{u}_i\frac{\partial\mathcal{I}_{LM}}{\partial x_i} = \frac{1}{T}\big(L_{ij}M_{ij} - \mathcal{I}_{LM}\big), \\ \frac{D\mathcal{I}_{MM}}{Dt} &\equiv \frac{\partial\mathcal{I}_{MM}}{\partial t} + \overline{u}_i\frac{\partial\mathcal{I}_{MM}}{\partial x_i} = \frac{1}{T}\big(M_{ij}M_{ij} - \mathcal{I}_{MM}\big). \end{aligned} \tag{6}$$

whose solutions yield

$$(C_s\Delta)^2 = \frac{\mathcal{I}_{LM}}{\mathcal{I}_{MM}}. \tag{7}$$

Here T is a time scale which represents the 'memory' of the Lagrangian averaging. Meneveau et al. (1996) proposed the following time scale:

$$T = \theta\Delta(\mathcal{I}_{LM}\mathcal{I}_{MM})^{(-1/8)}; \qquad \theta = 1.5. \tag{8}$$

This procedure for Lagrangian averaging has also been extended to the scale-similar model by Anderson and Meneveau (1999); Sarghini et al. (1999) and the scale-dependent dynamic model by Stoll and Porté-Agel (2006).

DYNAMIC LAGRANGIAN TIME SCALE

The time scale for Lagrangian averaging proposed by Meneveau et al. (1996) (henceforth, T_{LDSM}) contains an adjustable parameter which is typically chosen to be $\theta = 1.5$. This value was chosen based on the autocorrelation of $L_{ij}M_{ij}$ and $M_{ij}M_{ij}$ from DNS of forced isotropic turbulence. This arbitrariness is acknowledged to be undesirable by the authors and infact they document results of turbulent channel flow at $Re_\tau = 650$ to be marginally sensitive to the value of θ, with $\theta = 1.5$ appearing to yield the best results. You et al. (2007) tested three different values of the relaxation factor θ and concluded T_{LDSM} was 'reasonably robust' to the choice of θ for a $Re_\tau = 180$ channel flow. Over the years, choosing a value for θ has demanded significant consideration by many practitioners who have found the results to be sensitive to θ, especially in complex flows (Inagaki et al., 2002).

The extension of the Lagrangian averaging procedure to other models has also presented the same dilemma. In simulations of turbulent channel flow at $Re_\tau = 1050$ using a two-coefficient Lagrangian mixed model, Anderson and Meneveau (1999) and Sarghini et al. (1999) note that a different parameter in T_{LDSM} might be required for averaging the scale similar terms. Vasilyev et al. (2008) proposed extensions to the Lagrangian dynamic model for a wavelet based approach and used $\theta = 0.75$ for incompressible isotropic turbulence.

Park and Mahesh (2009) note that T_{LDSM} has a high dependence on the strain rate through the L_{ij} and M_{ij} terms. They however show that the time scale of the GIE near the wall and the channel centerline are similar. Thereby they argue that strain rate may not be the most appropriate quantity for defining a time scale for Lagrangian averaging of the GIE. It seems only natural that the averaging time scale should be the time scale of the quantity being averaged which in this case is the GIE. Park and Mahesh (2009) therefore, proposed a dynamic time scale T_{SC}, called "surrogate-correlation based time scale" T_{SC}.

However the Park and Mahesh (2009) formulation was in the context of a spectral structured solver, and considered their dynamic Lagrangian time scale model along with their proposed control-based Corrected DSM. The present work considers the dynamic Lagrangian time scale model in the absence of control-based corrections. This procedure for computing a dynamic Lagrangian time scale is extended to an unstructured grid framework.

Surrogate-correlation based time scale

Let us assuming knowledge of the local and instantaneous values of the GIE squared ($\mathcal{E} = \epsilon_{ij}\epsilon_{ij}$) at five consecutive events along a pathline:

$$\mathcal{E}^0 = \mathcal{E}(\mathbf{x}, t), \quad \mathcal{E}^{\pm 1} = \mathcal{E}(\mathbf{x} \pm \mathbf{u}\Delta t, t \pm \Delta t), \\ \mathcal{E}^{\pm 2} = \mathcal{E}(\mathbf{x} \pm 2\mathbf{u}\Delta t, t \pm 2\Delta t). \tag{9}$$

At each location, the following surrogate Lagrangian correlations for three separation times $(0, \Delta t, 2\Delta t)$ can be defined by computing a running time average upto the current time t_n:

$$\mathcal{C}(l\Delta t) = \sum_{t=0}^{t_n} \left(\frac{1}{5-l} \sum_{k=-2}^{2-l} (\mathcal{E}^{k,t} - \overline{\mathcal{E}}^t)(\mathcal{E}^{k+l,t} - \overline{\mathcal{E}}^t) \right) \\ \text{where} \quad \overline{\mathcal{E}}^t = \sum_{\tau=0}^{t_n} \left(\frac{1}{5} \sum_{k=-2}^{2} \mathcal{E}^{k,\tau} \right) \tag{10}$$

This leads to converged correlations after sufficiently long times and is a consistent and general method to compute the surrogate Lagrangian correlations. These correlations are then normalized by the zero-separation correlation $\mathcal{C}(0)$ to obtain

$$\rho(0) = 1, \quad \rho(\Delta t) = \frac{\mathcal{C}(\Delta t)}{\mathcal{C}(0)}, \quad \rho(2\Delta t) = \frac{\mathcal{C}(2\Delta t)}{\mathcal{C}(0)}. \tag{11}$$

An osculating parabola can be constructed passing through these three points and it can be described by

$$\rho(\delta t) = a(\delta t)^2 + b(\delta t) + 1 \tag{12}$$

where a, b can be written in terms of $\rho(0) = 1, \rho(\Delta t), \rho(2\Delta t)$ and Δt. Note that $\rho(\delta t)$ is an approximate correlation function (of separation time δt) for the true Lagrangian correlation. Thus the time scale based on the surrogate correlation T_{SC} is defined as the time when $\rho(\delta t) = 0$ *i.e.* the positive solution

$$T_{SC} = \frac{-b - \sqrt{b^2 - 4a}}{2a} \tag{13}$$

If the surrogate Lagrangian correlations $\mathcal{C}$ have enough samples, $1 > \rho(\Delta t) > \rho(2\Delta t)$ is satisfied which leads to $a < 0$. As a result T_{SC} is always positive. In the initial stages of a simulation, there are not enough time samples. $1 > \rho(\Delta t) > \rho(2\Delta t)$ may not be satisfied and a could be positive. In such cases, T_{SC} is obtained by constructing the osculating parabola to be of the form $1 + a(\delta t)^2$ and passing through either of the two points $\rho(\Delta t), \rho(2\Delta t)$:

$$T_{SC} = min(\frac{dt}{\sqrt{1 - \rho(\Delta t)}}, \frac{2dt}{\sqrt{1 - \rho(2\Delta t)}}) \tag{14}$$

The minimum of the time scales is chosen so that the solution has lesser dependence on past values and can evolve faster from the initial transient stage.

Lagrangian approximation

The proposed dynamic time scale requires the values of the Germano-identity error (GIE) squared $\mathcal{E}$ at five events along a pathline. Rovelstad et al. (1994) suggest the use of Hermite interpolation. Meneveau et al. (1996) use multilinear interpolation to obtain the values of $\mathcal{I}_{LM}$ and $\mathcal{I}_{MM}$ at a Lagrangian location. Both Hermite and multilinear interpolation get expensive in an unstructured grid setting. The use of an expensive interpolation method just to compute the time scale for Lagrangian averaging may be unnecessary. As a result, a simple material derivative relation as proposed by Park and Mahesh (2009) is used to approximate Lagrangian quantities in an Eulerian framework :

$$\frac{D\mathcal{E}}{Dt} = \frac{\partial \mathcal{E}}{\partial t} + \overline{u}_i \frac{\partial \mathcal{E}}{\partial x_i} \tag{15}$$

A simple first order in time and central second order in space, finite-volume approximation for the convective term is used to approximate values of $\mathcal{E}$ in eqn. 9 in terms of the local $\mathcal{E}(\mathbf{x}, t) = \mathcal{E}^{0,n}$ and $\mathcal{E}(\mathbf{x}, t - \Delta t) = \mathcal{E}^{0,n-1}$. The Green-Gauss theorem is used to express the convective term in conservative form and evaluate it as a sum over the faces of a computational volume.

NUMERICAL METHOD

Eq. 1 is solved by a numerical method developed by Mahesh et al. (2004) for incompressible flows on unstructured grids. The algorithm is derived to be robust without numerical dissipation. It is a finite volume method where the Cartesian velocities and pressure are stored at the centroids of the cells and the face normal velocities are stored independently at the centroids of the faces. A predictor-corrector approach is used. The predicted velocities

LES						
Case	Re_τ	$N_x \times N_y \times N_z$	Δx^+	Δz^+	Δy^+_{min}	$\Delta y_{cen}/\delta$
590c	590	$64 \times 64 \times 64$	58	29	1.6	0.08
590tl		$160 \times 84 \times (200, 100)$	23.2	9.3,18.5	1.8	0.04
1ktl	1000	$160 \times 84 \times (200, 100)$	39.3	15.8,31.4	3.1	0.04
2ktl	2000	$320 \times 120 \times (400, 200, 100)$	39.3	15.7,31.4,62.8	2.0	0.04
DNS						
Moser et al. (1999)	587	$384 \times 257 \times 384$	9.7	4.8	-	0.012
del Alamo et al. (2004)	934	$- \times 385 \times -$	11	5.7	-	-
Hoyas and Jimenez (2006)	2003	$- \times 633 \times -$	12	6.1	-	-

Table 1: Grid parameters for turbulent channel flow.

at the control volume centroids are first obtained and then interpolated to obtain the face normal velocities. The predicted face normal velocity is projected so that the continuity equation in eq. 1 is discretely satisfied. This yields a Poisson equation for pressure which is solved iteratively using a multigrid approach. The pressure field is used to update the Cartesian control volume velocities using a least-square formulation. Time advancement is performed using an implicit Crank-Nicolson scheme. The algorithm has been validated for a variety of problems over a range of Reynolds numbers (Mahesh et al., 2004). To improve results on skewed grids, the viscous terms and the pressure Poisson equation are treated differently. The Generalized Improved Deferred Correction method by Jang (2011) is used to calculate the viscous derivatives and the right-hand side of the pressure Poisson equation.

RESULTS: LAGRANGIAN DSM

The performance of the Lagrangian DSM with dynamic time scale T_{SC} (eq. 13) is evaluated by applying it to problems of increasing complexity: turbulent channel flow, cylinder flow, and flow past a marine propulsor attached to an upstream hull, operating in an off-design condition.

Turbulent channel flow

LES of a turbulent channel flow is performed at three Reynolds numbers; $Re_\tau = 590, 1000, 2000$ and different grid resolutions. Here $Re_\tau = u_\tau \delta/\nu$ where u_τ denotes friction velocity, δ channel half-width and ν viscosity. Table 1 lists the Re_τ and grid distribution for the various runs. All LES cases have a domain of $2\pi\delta \times 2\delta \times 2\pi\delta$ and a uniform spacing in x. The cases with 'tl' indicate that a 4 : 2 transition layer has been used in z along y. A transition layer allows transition between two fixed edge ratio computational elements. It allows a finer wall spacing to coarsen to a fixed ratio coarser outer region spacing. All other cases have a uniform spacing in z. Our LES results are compared to the DNS of Moser et al. (1999) for $Re_\tau = 590$, del Alamo et al. (2004) for $Re_\tau = 1000$, and Hoyas and Jimenez (2006) for $Re_\tau = 2000$ whose grid parameters are also included in the table for comparison. Note that the LES have employed noticeably coarse resolutions.

It will be shown that Lagrangian averaging using T_{SC} is able to predict better results and achieve the regularization effect of plane averaging while retaining spatial localization. For a given problem, as the grid becomes finer, the results obtained using different averaging schemes for DSM tend to become indistinguishable from one another. On a fine grid, the effect of averaging and Lagrangian averaging time scale is small. Case 590c is a very coarse grid and shows difference between the different averaging schemes. Fig. 1(a) shows that the mean velocity shows increasingly improving agreement with DNS as the averaging scheme changes from averaging along homogeneous directions (plane) to Lagrangian averaging using T_{LDSM} and finally T_{SC}. Note that though $\theta = 1.5$ was chosen for T_{LDSM}, using $\theta = 3.0$ produced results only marginally different (not shown). This just re-affirms that T_{LDSM} is marginally sensitive to the choice of θ for the given problem. The fact that Lagrangian averaging performs better than plane averaging has been demonstrated by Meneveau et al. (1996) and Stoll and Porté-Agel (2008). The present results show that using T_{SC} as the time scale for Lagrangian averaging yields as good as or even better results.

Stoll and Porté-Agel (2008) report that the Lagrangian averaged model using T_{LDSM} has approximately 8% negative values for ν_t compared to 40% for the locally smoothed (neighbor-averaged) model

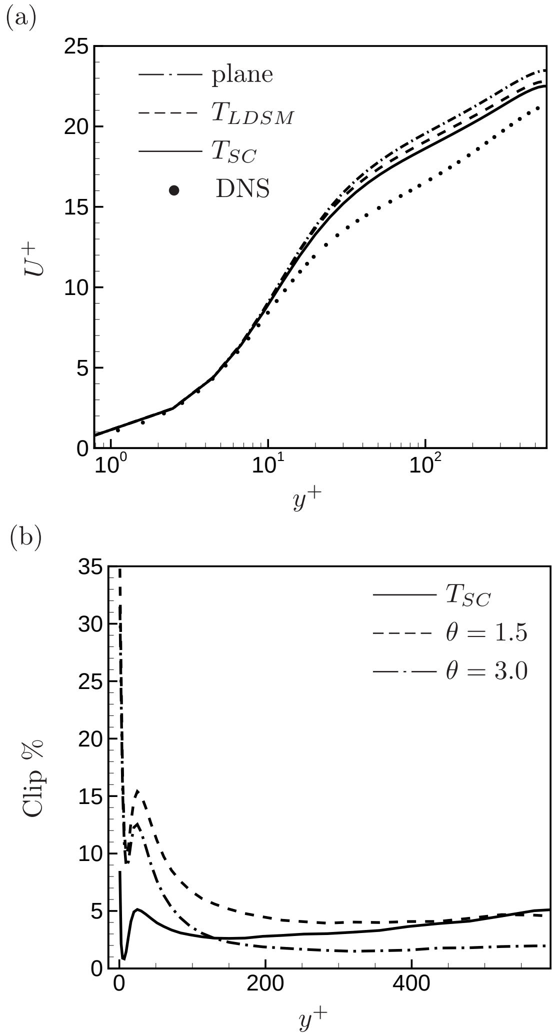

Figure 1: Comparison of time scales from case 590c: (a) mean velocity, (b) percentage of negative eddy viscosity.

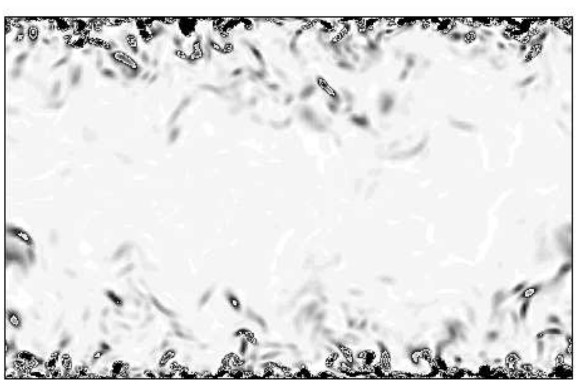

Figure 2: Turbulent channel flow : Instantaneous contours of Germano-identity error $g = (GIE/u_\tau^2)^2$, YZ plane, contours vary as $0 \leq g \leq 3$.

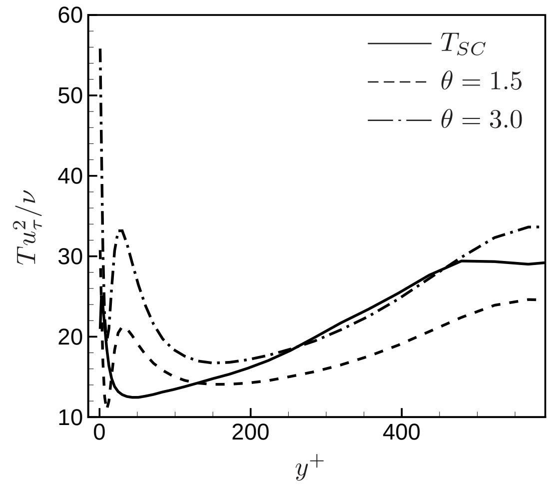

Figure 3: Comparison of time scales from case 590c.

in their simulations of stable atmospheric boundary layer. The percentage of time that ν_t is negative in our computations is shown in fig. 3(a). Plane averaged ν_t was never negative and hence is not plotted. Clearly, ν_t averaged using T_{SC} has the least number of negative values up until $y^+ \sim 100$ (which contains 50% of the points). Even after $y^+ \sim 100$, ν_t averaged using T_{SC} has lesser negative values than T_{LDSM} with $\theta = 1.5$. It is also observed that increasing θ reduced the number of negative values, as expected intuitively. Therefore, T_{SC} is able to achieve the smoothing effect of plane averaging while retaining spatial localization.

For this kind of relatively coarse near-wall resolution, GIE is expected to be high near the wall (as shown in fig. 2) and in addition, remain correlated longer because of the near-wall streaks. This results in a high correlation of GIE near the wall which leads to to a higher Lagrangian time scale. Consistent with this, fig. 3(b) shows that T_{SC} is much higher near the wall than T_{LDSM}. On closer inspection, T_{SC} is actually found to overlap with $T_{LDSM}, \theta = 3.0$ for almost half the channel width. For this particular computation, $\theta = 3.0$ is therefore a preferable alternative to $\theta = 1.5$. This makes it entirely reasonable to suppose that other flows might prefer some other θ than just 1.5. The dynamic procedure used in this paper alleviates this problem.

It must be noted that computing a dynamic T_{SC} for Lagrangian averaging the DSM terms does not incur a significant computational overhead. For case 590c, the total computational time required for computing T_{SC} and then using it for Lagrangian averaging of the DSM terms is just 2% more than that when no averaging is performed.

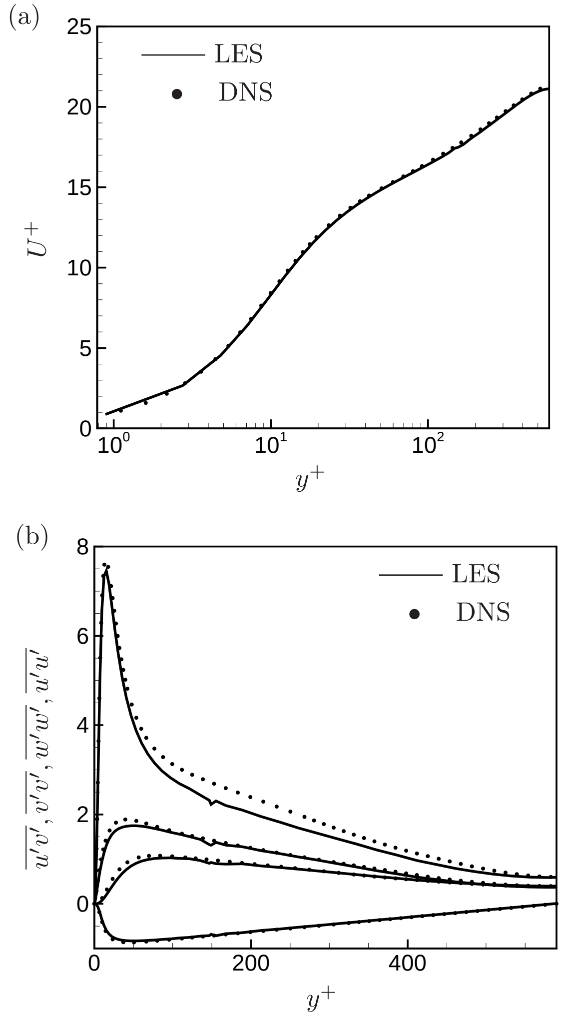

Figure 4: Turbulent channel flow : Case 590tl (a) mean velocity, (b) rms velocity fluctuations.

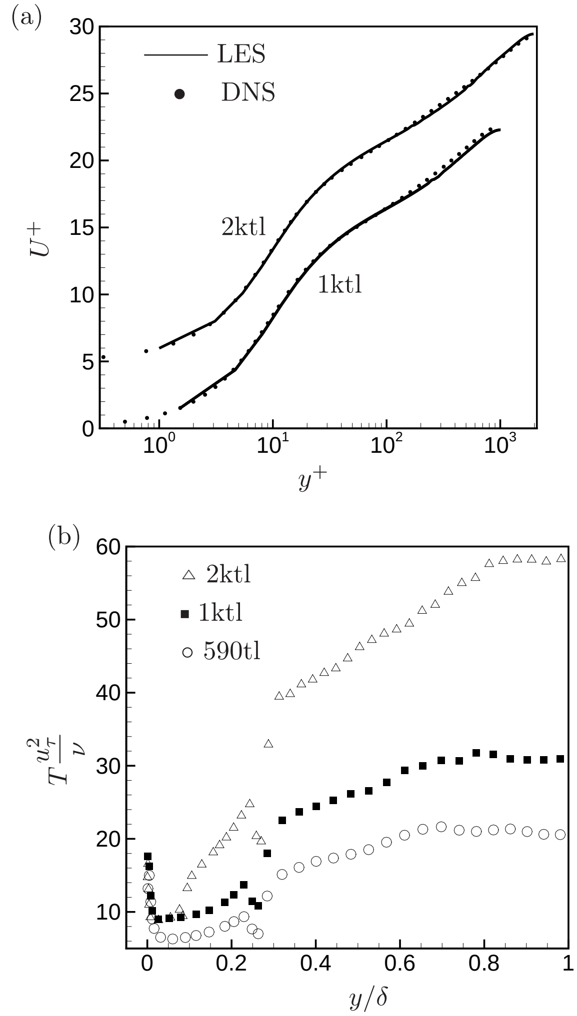

Figure 5: Turbulent channel flow : (a) mean velocity, (b) Lagrangian time scales T_{SC}.

A wall-resolved LES is performed using an unstructured zonal grid, which has a transition layer in Z along Y (case 590tl). Figs. 4(a)-(b) show that the results are in good agreement. The statistics (fig. 4(b)) have a small kink around $y^+ \sim 140$ where the grid transitions. This kink in the statistics is an artifact of numerical discretization and grid skewness and is present even when no SGS model is used.

The proposed model (eq. 13) is applied to turbulent channel flow at higher Reynolds numbers of $Re_\tau = 1000$ and $Re_\tau = 2000$. The grid used for case 1ktl is the same as used for case 590tl and hence the resolution in wall units is almost twice as coarse, as shown in table 1. The grid used for case 2ktl is based on similar scaling principles as case 590tl, which is to enable a wall-resolved LES. Hence, it has 2 transition layers to coarsen from a fine near-wall Δz to a coarser outer region Δz. Fig. 5(a) shows good agreement for the mean velocity which indicates that the wall stress is well predicted. Fig. 5(b) compares the computed Lagrangian time scales for the three cases - 590tl, 1ktl and 2ktl . With increasing Reynolds number, the correlation of GIE increases which results in increasing T_{SC}. Overall, the results indicate that the Lagrangian DSM with T_{SC} works well for high Reynolds number wall-bounded flows on grids where non-orthogonal elements are present and plane averaging is not straightforward.

Flow past a circular cylinder

The Lagrangian DSM with dynamic time scale T_{SC} (eq. 13) is applied to flow past a circular cylinder. LES is performed in the turbulent regime at $Re_D = 3900$ (based on freestream velocity U_∞ and cylinder diameter D). The computational domain and

	$<C_D>$	$\sigma(C_L)$	St	$-C_{P_b}$	θ°_{sep}	L_{rec}/D
T_{SC}	1.01	0.139	0.210	1.00	88.0	1.40
T_{LDSM}	0.99	0.135	0.208	1.00	87.0	1.63
Kravchenko and Moin (2000)	1.04	-	0.210	0.94	88.0	1.35
Experiment (taken from Mahesh et al. (2004))	0.99	-	0.215	-	86.0	1.40

Table 2: Flow parameters at $Re_D = 3900$. Legend for symbols : mean drag coefficient $<C_D>$, rms of drag and lift coefficient $(\sigma(C_D), \sigma(C_L))$, Strouhal number St and base pressure C_{P_b}, separation angle θ°_{sep}, recirculation length L_{rec}/D.

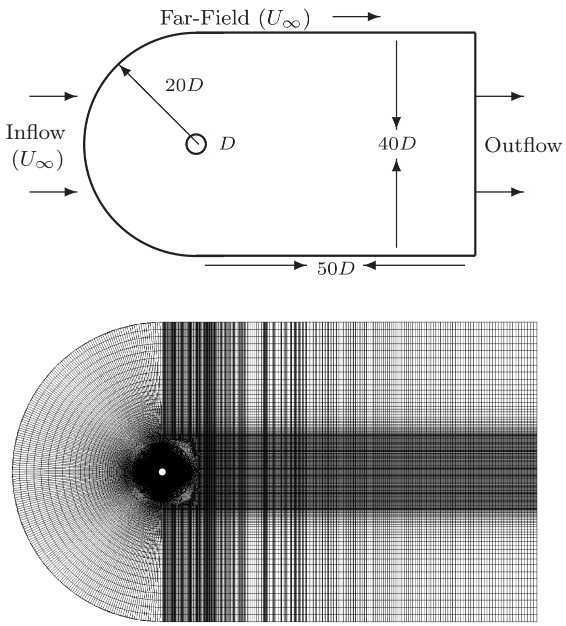

Figure 6: Computational domain with boundary conditions and grid for a cylinder.

boundary conditions used the simulation are shown in fig. 6. The domain height is $40D$, spanwise width πD and extends $50D$ downstream and $20D$ upstream of the center of the cylinder. An unstructured grid of quadrilaterals is first generated in a plane, such that computational volumes are clustered in the boundary layer and the wake. This two-dimensional grid is then extruded in the spanwise direction to generate the three-dimensional grid; 80 spanwise planes are used for both the simulations and periodic boundary conditions imposed in those directions. Uniform flow is specified at the inflow, and convective boundary conditions are enforced at the outflow. The smallest computational volume on any spanwise station of the cylinder is of the size $2.0e^{-3}D \times 5.2e^{-3}D$ but stretches to $3.9e^{-2}D \times 2.9e^{-2}D$ at a downstream location of $5D$.

Fig. 7 shows that the instantaneous GIE also

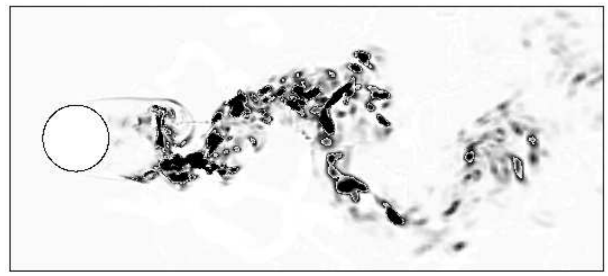

Figure 7: Cylinder flow - $Re_D = 3900$: Instantaneous contours of Germano-identity error whose contours vary as: $0 \leq (GIE/U^2_\infty)^2 \leq 0.001$.

follows the pattern of the Karman vortex street. The top shear layer can be seen to roll up (within one diameter) to form the primary vortex. The GIE is highest in the turbulent shear layers where scales are smaller. Dowsntream, as the turbulence becomes more developed and scales become bigger, GIE diminishes. As the grid becomes coarser downstream, DSM plays a more dominant role, providing a higher value of ν_t which reduces GIE. It appears that GIE follows the dominant structures in the flow and hence it is reasonable that Lagrangian averaging uses a time scale based on a correlation of the GIE.

To compare performance of different Lagrangian averaging based methods, results are computed using both the proposed surrogate correlation based time scale T_{SC} and the standard time scale T_{LDSM}. Integral quantities using T_{SC} show good agreement with the B-spline computation of Kravchenko and Moin (2000) and the experiments of Lourenco & Shih (taken from Mahesh et al. (2004)) as shown in table 2. Note that T_{LDSM} also shows good agreement for the wall quantities; however, L_{rec}/D which depends on the near-field flow, shows discrepancy. This points towards a difference in the values of the time scales away from the cylinder.

There have been numerous studies comparing the time averaged statistics for flow over a cylinder. However different authors have used varying

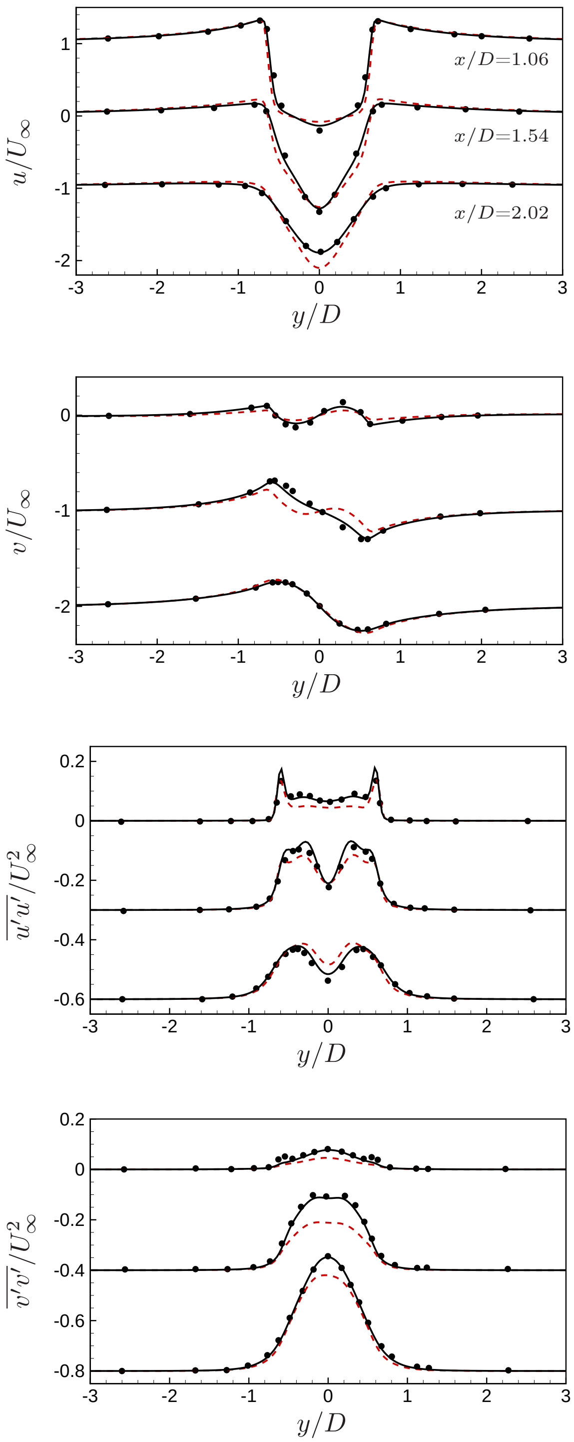

Figure 8: Vertical profiles at streamwise stations downstream of the cylinder at $Re_D = 3900$. ——— : T_{SC}; - - - - : T_{LDSM}; • : B-spline solution of Kravchenko and Moin (2000).

time periods for averaging. Franke and Frank (2002) studied this issue in detail and noted that more than

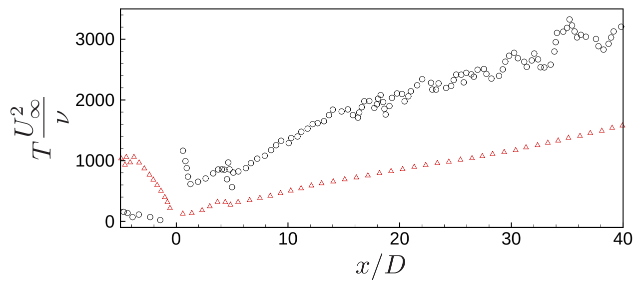

Figure 9: Downstream evolution of the Lagrangian time scale on the centerline of the cylinder wake at $Re_D = 3900$. ○ : T_{SC}; △ : T_{LDSM}.

40 shedding periods are required to obtain converged mean flow statistics in the neighborhood of the cylinder. Tremblay et al. (2000) averaged over 60 shedding cycles in their DNS using an immersed boundary method. In the current work, statistics are obtained over a total time of $404D/U_\infty$ ($\sim$ 85 shedding periods) and then averaged over the spanwise direction for more samples. Converged mean flow and turbulence statistics using T_{SC} show good agreement with the B-spline computations of Kravchenko and Moin (2000) upto $x/D = 2$ as shown in figs. 8. Results using T_{LDSM} are also shown for comparison. Difference in the statistics between the two time scales seem to be significant in the near-wake.

These differences could be attributed to the contribution of the SGS model. Differences in the computed eddy viscosity arise due to different time scales for Lagrangian averaging of the DSM terms. Both T_{SC} and T_{LDSM} are found to increase almost linearly downstream after $x/D > 5$ as shown in fig. 9, though for different reasons. Based on the surrogate correlation of the GIE, increasing T_{SC} is consistent with the flow structures becoming bigger as they advect downstream. Whereas, strong dependence of T_{LDSM} on the strain rate gives it a linear profile both ahead of and behind the cylinder. It can be argued that perhaps a different value of the relaxation factor θ would be more appropriate for this flow. In fact, fig. 9 makes it apparent that if T_{LDSM} were to be doubled, its value would be closer to that of T_{SC}. Again, it can be crudely estimated that scaling the value of θ by a factor of two or so ($\theta \geq 3.0$) will result in T_{LDSM} being close to T_{SC} after $x/D > 5$. However, it is clear that T_{LDSM} would still not show the appropriate trend ahead of the cylinder and in the recirculation region. Note that, as expected, T_{SC} is high just behind the cylinder ($x/D \sim 1$) in the recirculation region and low in the high acceleration region ahead of the cylinder.

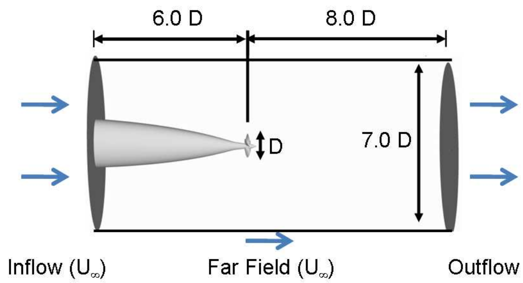

(a)

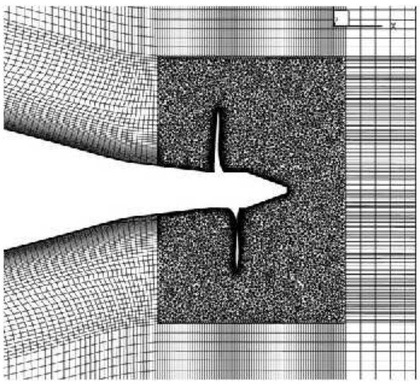

(b)

Figure 10: (a) Computational domain and boundary conditions on domain boundaries, (b) XY plane of grid for propeller with hull.

Marine propeller in crashback

Propeller crashback is an off-design operating condition where the marine vessel is moving forward but the propeller rotates in the reverse direction to slow down or reverse the vessel. The crashback condition is dominated by the interaction of the free stream flow with the strong reverse flow from reverse propeller rotation; this interaction forms an unsteady vortex ring around the propeller. Crashback is characterised by highly unsteady forces and moments on the blades due to large flow separation and hence is a very challenging flow for simulation. Vyšohlid and Mahesh (2005, 2006) performed one of the first LES of a marine propeller in crashback. Chang et al. (2008) coupled the unsteady blade loads with a structural solver to predict shear stress and bending moment on the propeller blades during crashback. Jang and Mahesh (2010, 2012) studied crashback at three advance ratios and proposed a flow mechanism. Verma et al. (2011, 2012) explained the effect of an upstream hull on a marine propeller in

(a)

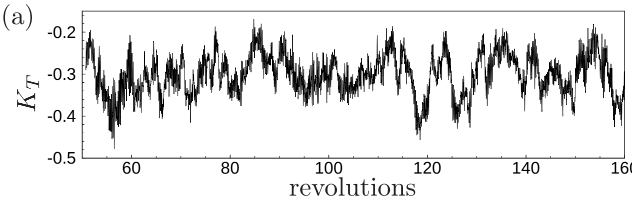

(b)

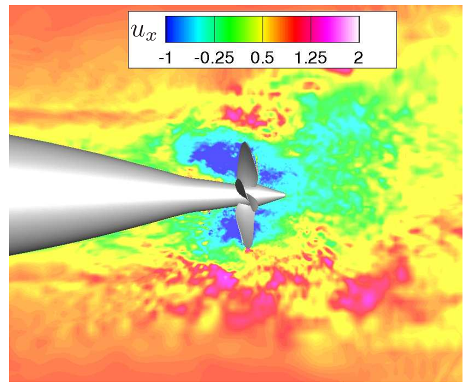

Figure 11: (a) Time history of unsteady thrust K_T on the propeller blades, (b) Instantaneous axial velocity u_x.

crashback. These simulations were performed using locally-regularized DSM.

In the current work, LES of a marine propeller, attached to an upstream submarine hull is performed using the Lagrangian averaged DSM with the proposed dynamic time scale (eq. 13). Preliminary results are shown at a Reynolds number of $Re = 480,000$ and advance ratio of $J = -0.7$. Here

$$Re = \frac{UD}{\nu} \quad \text{and} \quad J = \frac{U}{nD}$$

where U is the free-stream velocity, n is the propeller rotational speed, and D is the diameter of the propeller disk.

Simulations are performed in a frame of reference that rotates with the propeller with the absolute velocity vector in the inertial frame. The computational domain is a cylinder with diameter $7.0D$ and length $14.0D$ as shown in fig. 10(a). Free-stream velocity boundary conditions are specified at the inlet and the lateral boundaries. Convective boundary conditions are prescribed at the exit. Boundary conditions on the rotor part, blades and hub are specified as $u = \omega \times r$, where $\omega = 2\pi n$ and r is the radial distance from the propeller center. No-slip boundary conditions are imposed on the hull body. An unstructured grid with 7.3 million cvs is used as shown in fig. 10(b). The propeller surface is meshed with quadrilateral elements. Four layers of prisms

	$\langle K_T \rangle$	$\sigma(K_T)$	$\langle K_Q \rangle$	$\langle K_S \rangle$	$\sigma(K_S)$
LES	-0.358	0.113	-0.067	0.046	0.024
Experiment (Bridges et al., 2008)	-0.340	0.085	-0.060	0.044 - 0.048	0.019 - 0.021

Table 3: Propeller in crashback: Computed and experimental values of mean and rms of coefficient of thrust K_T, torque K_Q and side-force K_S on propeller blades.

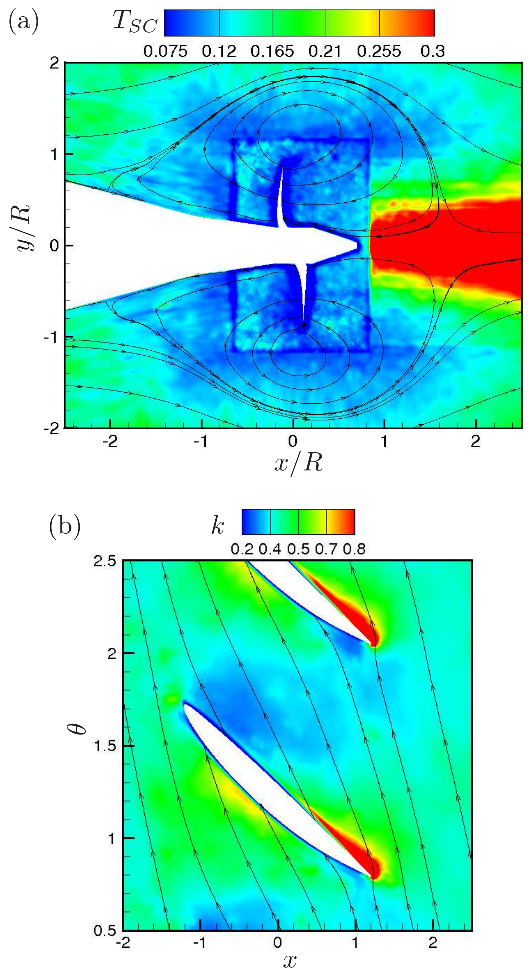

Figure 12: **J=-0.7**. (a) Contours of time scale T_{SC} with streamlines, (b) Time averaged turbulent kinetic energy field with streamlines at a constant radial plane of $r/R = 0.4$.

are extruded from the surface with a minimum wall-normal spacing of $0.0017D$ and a growth ratio of 1.05. A compact cylindrical region around the propeller is meshed with tetrahedral volumes while the rest of the domain is filled with hexahedral volumes.

The forces and moments are non-dimensionalized by using propulsive scaling. The time history of the coefficient of thrust K_T shows the unsteadiness of the predicted thrust (axial force) on the propeller blades due to the highly unsteady flow field around the propeller (fig. 11). Reverse rotation of the propeller induces reverse flow into the propeller disk, which interacts with the wake of the upstream hull, rolling up into a vortex ring. The unsteadiness of the forces is due to the fact that the propeller blades experience highly separated flow and an unsteady vortex ring.

Time averaged statistics of flow field are computed over 70 propeller rotations as a preliminary result. Table 3 shows the predicted mean and rms of the unsteady forces and moments on the blades to be in reasonable agreement with the experiment of Bridges et al. (2008). Fig. 12(a) shows an xy plane slice cutting the center and along the length of the hull. The time averaged contours of the Lagrangian time scale T_{SC} along with streamlines are plotted. The streamlines reveal a vortex ring, centered near the blade tip. A small recirculation zone is formed on the hull ($x/R \sim -2$) due to the interaction of the wake of the hull with the reverse flow induced into the propeller disk by the reverse rotation of the propeller. Compared to $J = -1.0$ (Verma et al., 2012), this recirculation zone is much smaller and located further upstream of the blades. This is consistent with a higher rotational rate of the propeller inducing a higher reverse flow into the propeller disk.

The Lagrangian time scale T_{SC} is seen to be physically consistent with the flow. It is high in the low-momentum wake behind the propeller where flow structures are expected to be more coherent. T_{SC} is low in the unsteady vortex ring region around the propeller blades. The cylindrical region around the blades is where the grid transitions from tetrahedral to hexahedral volumes. Turbulent kinetic energy (k) is a measure of three-dimensional unsteadiness and turbulence in the flow. Fig. 12(b) shows the resolved turbulent kinetic energy within the blade passage at a radial plane of $r/R = 0.4$. k is highest near the leading edge of the blades, related to the unsteadiness caused by the reverse flow separating at the sharp leading edge. The performance of T_{SC} for such complex flows is encouraging.

REYNOLDS STRESS CONSTRAINED WALL MODEL

The Lagrangian averaged DSM with a dynamic time scale gives better results over existing averaged DSM methods. However, it does not solve the wall modeling problem. Fig. 13 shows that the GIE from the 3 cases 590tl, 1ktl, and 2ktl (which use relatively 'wall-resolved' grids) is still high in the near-wall region; the error increases as the grid coarsens. This is indicative of greater SGS modeling errors near the wall, especially when coarser near-wall grids are employed for LES. It is well known that LES with simple eddy viscosity model works poorly for wall-bounded flows (Piomelli et al., 1996; Templeton et al., 2006; Park and Mahesh, 2008a). This is primarily due to the fact that near the wall, flow structures scale in viscous units. If the near-wall grid is fashioned to resolve the large or integral length scales of the flow, these near-wall structures remain unresolved. Moreover, near-wall flow structures tend to be anisotropic and simple SGS models fail to accurately represent the turbulent stress near the wall. It has been estimated that the grid requirement for a wall-resolved LES scales as Re_τ^2 (Baggett et al., 1997); comparable to that for a DNS which scales as $Re_\tau^{9/4}$. In order to overcome this severe resolution requirement, various wall modeling approaches have been suggested and summarized in various review articles (Piomelli and Balaras, 2002; Piomelli, 2008). One such approach is that of hybridizing Reynolds Averaged Navier-Stokes (RANS) and LES formulations. The present study is motivated by (1) the inherent limitations of the existing hybrid RANS-LES methodologies and (2) the challenges in implementing a robust hybrid RANS-LES framework for complex flows on unstructured grids.

Detached-Eddy Simulation (DES) by Spalart et al. (1997) is a widely used approach for high Reynolds number flows. The idea behind DES is to compute the boundary layer using RANS and use LES away from the wall (in the 'separated' region). Many hybrid RANS-LES type formulations also use essentially what is a RANS-type eddy viscosity near the wall and 'blend' it with LES eddy viscosity away from the wall. The basic idea behind the present work can be summarized as:

- Using a RANS model directly in the near-wall region produces excessive dissipation (Park and Mahesh, 2008b). A less dissipative "subgrid scale model" is needed which leads solution to a target quantity prescribed from external data only in the mean sense. This target quantity may be the wall stress, Reynolds stress or mean velocity.
- The intention is to perform LES in the whole computational domain using a simple yet robust wall model. In general, LES is superior to RANS even with coarse resolutions away from the wall. The external Reynolds stress constraint should be imposed in a limited region (near the wall) where LES is expected to be erroneous.

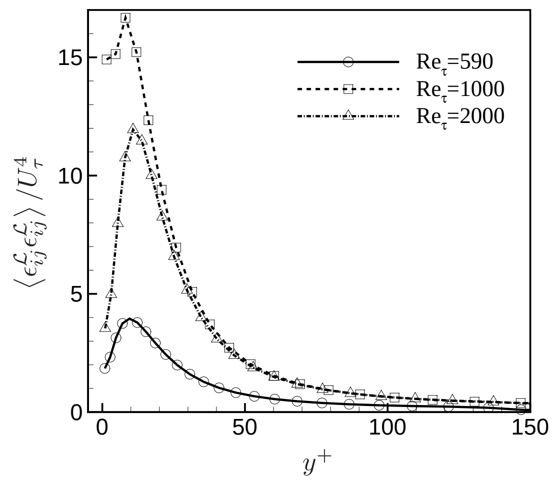

Figure 13: Turbulent channel flow: Germano-identity error.

A hybrid dynamic SGS model constrained by externally prescribed Reynolds stress is formulated in the next section. The proposed model is then applied to turbulent channel flow at various Reynolds numbers and grid distributions.

A CONSTRAINED DYNAMIC SGS MODEL

An advantage of the dynamic procedure is that various terms can be easily incorporated to form dynamic mixed models. Ghosal et al. (1995) proposed a dynamic localization model by including a non-negative constraint on the model coefficient. Shi et al. (2008) imposed an energy dissipation constraint on the dynamic mixed similarity model. In the present work, Reynolds stress is considered to be provided as an externally prescribed constraint. More particularly, only a time average of the Reynolds stress needs to be provided and hence it could be sourced from RANS, DNS, experimental statistics or even empirical closures/fits. A simple and efficient hybrid SGS model was first proposed by Park and Mahesh (2008b) that combines the dynamic Smagorinsky model (DSM) approach and Reynolds stress constraints. However, they used averaging along homogeneous directions in the context of a spectral, structured solver. The current work extends this formulation to unstructured grids without averaging along homogeneous directions. A Lagrangian averaged version of this formulation is used to show improved results for turbulent channel flow in the next section.

Formulation

For simplicity, let us assume that Reynolds stress $\mathcal{R}_{ij} = \langle u_i u_j \rangle_E - \langle u_i \rangle_E \langle u_j \rangle_E$ is given from an external RANS solution. Here, $\langle \cdot \rangle_E$ denotes an ensemble average, which is equivalent to $\langle \cdot \rangle_t =$ time averaging. The ensemble average of SGS stress satisfies

$$\underbrace{\langle \overline{u}_i \overline{u}_j \rangle_E - \langle \overline{u}_i \rangle_E \langle \overline{u}_j \rangle_E}_{resolved} + \underbrace{\langle \tau_{ij} \rangle_E}_{SGS} = \mathcal{R}_{ij} \tag{16}$$

However, imposition of this condition on unsteady simulations is not straightforward. Consider therefore, an instantaneous version of (16) with SGS model τ_{ij}^M:

$$\epsilon_{ij}^{\mathcal{R}} = \overline{u}_i \overline{u}_j - U_i U_j + \tau_{ij}^M - \mathcal{R}_{ij}, \tag{17}$$

where $\epsilon_{ij}^{\mathcal{R}}$ is the error (and $\mathcal{R}$ denotes RANS), and

$$U_i = \frac{1}{T} \int_0^T \overline{u}_i dt \equiv \langle \overline{u}_i \rangle_T \tag{18}$$

is cumulative, ensemble–averaged velocity up to current time T. When T is sufficiently large, $\epsilon_{ij}^{\mathcal{R}}$ in (17) represents deviation from (16) due to SGS modeling error. Thus, the minimization of $\epsilon_{ij}^{\mathcal{R}}$ seems to be a proper RANS constraint.

On the other hand, error from the Germano identity is

$$\epsilon_{ij}^{\mathcal{L}} = T_{ij} - \widehat{\tau_{ij}^M} - L_{ij}, \tag{19}$$

where $\mathcal{L}$ denotes 'LES'. Then, cost function to be minimized can take the form

$$\mathcal{J}(C_s) = \int_\Omega \epsilon_{ij}^{\mathcal{L}} \epsilon_{ij}^{\mathcal{L}} d\mathbf{x} + \omega^{\mathcal{R}} \int_\Omega \left\langle \epsilon_{ij}^{\mathcal{R}} \right\rangle_T \left\langle \epsilon_{ij}^{\mathcal{R}} \right\rangle_T d\mathbf{x}, \tag{20}$$

where we consider a one–parameter SGS model $\tau_{ij}^M = \tau_{ij}^M(C_s)$, Ω is the domain, and $\omega^{\mathcal{R}}$ is the weight function for RANS constraints.

Then, the optimal C_s is given by

$$\delta \mathcal{J}(C_s) = \int_\Omega \frac{\partial}{\partial C_s} \left[\epsilon_{ij}^{\mathcal{L}} \epsilon_{ij}^{\mathcal{L}} + \omega^{\mathcal{R}} \left\langle \epsilon_{ij}^{\mathcal{R}} \right\rangle_T \left\langle \epsilon_{ij}^{\mathcal{R}} \right\rangle_T \right] \delta C_s d\mathbf{x} = 0, \tag{21}$$

which implies that

$$\frac{\partial}{\partial C_s} \left[\epsilon_{ij}^{\mathcal{L}} \epsilon_{ij}^{\mathcal{L}} + \omega^{\mathcal{R}} \left\langle \epsilon_{ij}^{\mathcal{R}} \right\rangle_T \left\langle \epsilon_{ij}^{\mathcal{R}} \right\rangle_T \right] = 0. \tag{22}$$

Eq. (22) is a general relation that can be used for complex flows and one–parameter SGS models.

Note that the above relation can be easily modified to be applicable with the homogeneous averaged and the Lagrangian averaged DSM (eq. 5). Let us consider $\epsilon_{ij}^{\mathcal{L}}$ and $\epsilon_{ij}^{\mathcal{R}}$ for the Smagorinsky model (SM) (Smagorinsky, 1963)

$$\tau_{ij} - \frac{1}{3}\tau_{kk} = -2C_s \Delta^2 |\overline{S}| \overline{S}_{ij}, \tag{23}$$

where $|\overline{S}| = \sqrt{2\overline{S}_{ij}\overline{S}_{ij}}$.

First, Germano identity error (GIE) is

$$\begin{aligned} \epsilon_{ij}^{\mathcal{L}} &= C_s \left(-2\widehat{\Delta}^2 |\widehat{\overline{S}}| \widehat{\overline{S}}_{ij} + 2\Delta^2 \widehat{|\overline{S}| \overline{S}}_{ij} \right) - L_{ij} \\ &\equiv C_s M_{ij} - L_{ij}. \end{aligned} \tag{24}$$

Here, all tensors are inherently or made traceless. Therefore, the first part in the bracket of Eq. (22) is

$$\epsilon_{ij}^{\mathcal{L}} \epsilon_{ij}^{\mathcal{L}} = C_s^2 M_{ij} M_{ij} - 2C_s L_{ij} M_{ij} + L_{ij} L_{ij}, \tag{25}$$

which leads to

$$\frac{\partial \epsilon_{ij}^{\mathcal{L}} \epsilon_{ij}^{\mathcal{L}}}{\partial C_s} = 2C_s M_{ij} M_{ij} - 2L_{ij} M_{ij}. \tag{26}$$

Obviously, equating eq. (26) to zero results in the standard DSM (Germano et al., 1991; Lilly, 1992).

Next, RANS Reynolds–stress reconstruction error (eq. 17) is considered:

$$\begin{aligned} \left\langle \epsilon_{ij}^{\mathcal{R}} \right\rangle_T &= \left\langle r_{ij} - 2C_s \Delta^2 |\overline{S}| \overline{S}_{ij} - \mathcal{R}_{ij} \right\rangle_T \\ &= \langle r_{ij} \rangle_T - 2\Delta^2 C_S \left\langle |\overline{S}| \overline{S}_{ij} \right\rangle_T - \mathcal{R}_{ij} \\ &\approx \underbrace{\langle r_{ij} \rangle_T - \mathcal{R}_{ij}}_{A_{ij}} - \underbrace{2\Delta^2 \left\langle |\overline{S}| \overline{S}_{ij} \right\rangle_T}_{B_{ij}} C_s \\ &\equiv A_{ij} - B_{ij} C_s. \end{aligned} \tag{27}$$

where $r_{ij} = \overline{u}_i \overline{u}_j - U_i U_j$ and C_s is assumed constant in time. Similar to $\epsilon_{ij}^{\mathcal{L}}$, the second part of eq. (22) is

$$\frac{\partial \left\langle \epsilon_{ij}^{\mathcal{R}} \right\rangle_T \left\langle \epsilon_{ij}^{\mathcal{R}} \right\rangle_T}{\partial C_s} = 2C_s B_{ij} B_{ij} - 2A_{ij} B_{ij}. \tag{28}$$

Inserting eqs. (26) and (28) in eq. (22) yields C_s as

$$C_s = \frac{L_{ij} M_{ij} + \omega^{\mathcal{R}} A_{ij} B_{ij}}{M_{ij} M_{ij} + \omega^{\mathcal{R}} B_{ij} B_{ij}}. \tag{29}$$

LES							
Case	Re_τ	$N_x \times N_y \times N_z$	$L_x/\delta \times L_z/\delta$	Δx^+	Δz^+	Δy^+_{min}	$\Delta y_{cen}/\delta$
590un	590	$160 \times 66 \times (150, 100)$	$2\pi \times \pi$	23.2	12.4,18.5	3.5	0.05
1kun	1000	$160 \times 70 \times (150, 100)$	$2\pi \times \pi$	39.3	21,31.4	4	0.05
2kun	2000	$160 \times 74 \times (150, 100)$	$2\pi \times \pi$	78.5	42,63	4	0.05
DNS							
Moser et al. (1999)	587	$384 \times 257 \times 384$	$2\pi \times \pi$	9.7	4.8	-	0.012
del Alamo et al. (2004)	934	$- \times 385 \times -$	$8\pi \times 3\pi$	11	5.7	-	-
Hoyas and Jimenez (2006)	2003	$- \times 633 \times -$	$8\pi \times 3\pi$	12	6.1	-	-

Table 4: Grid parameters for turbulent channel flow.

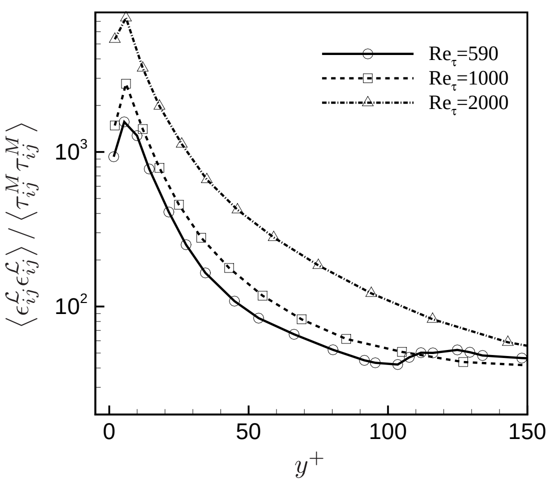

Figure 14: Turbulent channel flow: Germano-identity error normalized by modeled subgrid stress.

Dynamic determination of $\omega^{\mathcal{R}}$

In principle, the above expression for C_s (eq. 29) is applicable throughout the flow. However, as menioned earlier, the intention is to apply the external Reynolds stress constraint only in a limited region where LES is expected to be erroneous. We propose the Germano-identity error (eq. 19) as a measure of accuracy of LES utilizing a dynamic Smagorinsky SGS model. Figs. 2 and 13 show respectively, that the instantaneous and time-averaged GIE is very high near the wall, so that the validity of the Smagorinsky SGS model (eq. 23) in this region can be questioned. The external Reynolds stress constraint should be active in such regions where the GIE is deemed too high; to be determined by the weight function $\omega^{\mathcal{R}}$. Note that, to transition from RANS to LES, DES uses purely grid parameters such as the wall distance and local grid spacing; its variants incorporate some flow information. The current proposal to use GIE is explicitly dependent on the flow and the underlying SGS model.

Let us denote $\mathcal{E} = \epsilon_{ij}^{\mathcal{L}} \epsilon_{ij}^{\mathcal{L}} / \tau_{ij}^M \tau_{ij}^M$ as the Germano-identity error normalized by the modeled SGS stress (fig. 14). The weight function $\omega^{\mathcal{R}}$ is then proposed to be of the form,

$$\omega^{\mathcal{R}} = C_\omega \max\left(\mathcal{E} - \mathcal{E}_{\rm t}, 0\right), \tag{30}$$

where C_ω is a scaling coefficient and $\mathcal{E}_t$ is the threshold value. Nominally, $\omega^{\mathcal{R}}$ is determined using $C_\omega = 0.1$ and $\mathcal{E}_t = 100$ is chosen to impose the constraints in the near-wall region.

Hence $\omega^{\mathcal{R}} \neq 0$ implies the Reynolds stress constraint is active only in the region where the normalized Germano-identity error $\mathcal{E}$ exceeds a certain threshold $\mathcal{E}_t$. Fig. 14 shows that the constraint would be active only in the near-wall region (for cases 590un, 1kun, and 2kun as described in table 4). Obviously, $\omega^{\mathcal{R}} = 0$ retrieves the standard DSM.

RESULTS: WALL MODEL

The goal of wall modeling is to relax the grid requirement scaling with Reynolds number. DES hopes to achieve this by operating on a RANS near-wall grid where the wall-parallel spacing is large compared to the boundary-layer thickness ($\Delta_\parallel \gg \delta$) but the wall-normal grid spacing requirement is stricter ($\Delta^+_{\perp,w} \sim O(1)$). Nikitin et al. (2000) followed this guideline for their DES of channel flow and showed results with $\Delta_\parallel = 0.1\delta$ and $\Delta y^+_w < 1$. Further savings could be obtained by relaxing the wall-normal grid spacing requirement. When the first off-wall grid point is in the log layer, the filter width is much larger than the local turbulent integral scales. Hence, wall stress models are required to compensate for the SGS modeling errors in this region. Nicoud et al. (2001) and Templeton et al. (2005) use walls stress models on coarse LES grids.

Our motivation is to perform LES at high Reynolds numbers using no-slip boundary conditions at the wall with a slightly relaxed near-wall grid requirement. Results are shown with grids where the first off-wall grid point is in the viscous layer ($\Delta y_w^+ \leq 5$). In what follows, DSM denotes Lagrangian averaged Dynamic Smagorinsky Model and CDSM denotes Constrained DSM (with Lagrangian averaging for the DSM terms) which is the proposed constrained model (eq. 29). CDSM is applied to turbulent channel flow at three Reynolds numbers; $Re_\tau = 590, 1000, 2000$ to show improvement over DSM. Table 4 lists the Re_τ and grid distribution for the various runs. All LES cases have uniform spacing in x; 'un' indicates that an unstructured grid has been used near the wall in the spanwise direction (z) to allow flexibility in the near-wall grid while maintaining a fixed coarse outer-region grid. The LES results are compared to DNS whose grid parameters are also included in the table for comparison. The numerical method used is the same as described earlier.

Fig. 15 shows results for case 590un with parameters $C_\omega = 0.1$, $\mathcal{E}_t = 100$ and Reynolds shear stress from the DNS of Moser et al. (1999) as the constraint. CDSM shows marginal improvement over DSM for mean and rms streamwise velocity at this grid resolution. With CDSM, resolved shear stress (fig. 15(c)) reduces slightly near the wall but is compensated by higher SGS stress such that the total shear stress is closer to the DNS constraint. This establishes that the constrained formulation CDSM (i) is successful in constraining the total shear stress to an externally provided constraint in the mean and (ii) shows improvement over DSM.

However the improvement is significant when the near-wall grid resolutions for the LES are coarse. To this end, simulations are performed at $Re_\tau = 1000$ using both DSM and CDSM with a coarser Δz^+ and Δx^+. Fig. 16 shows results at $Re_\tau = 1000$ from case 1kun with parameters $C_\omega = 0.1$, $\mathcal{E}_t = 100$. The CDSM results for mean and rms u-velocity are in good agreement with unfiltered DNS. As with case 590un, fig. 16(c) shows that with CDSM, the resolved shear stress reduces slightly near the wall but is compensated by higher SGS stress; the total Reynolds shear stress computed is closer to the imposed constraint especially near the wall which is where the constraint is being activated due to high GIE. CDSM predicts a higher near-wall SGS stress due to higher eddy viscosity near the wall as shown in fig. 17(a). The constrained minimization of the GIE with an external constraint also reduces the GIE near the wall (fig. 17(b), right side, red) for

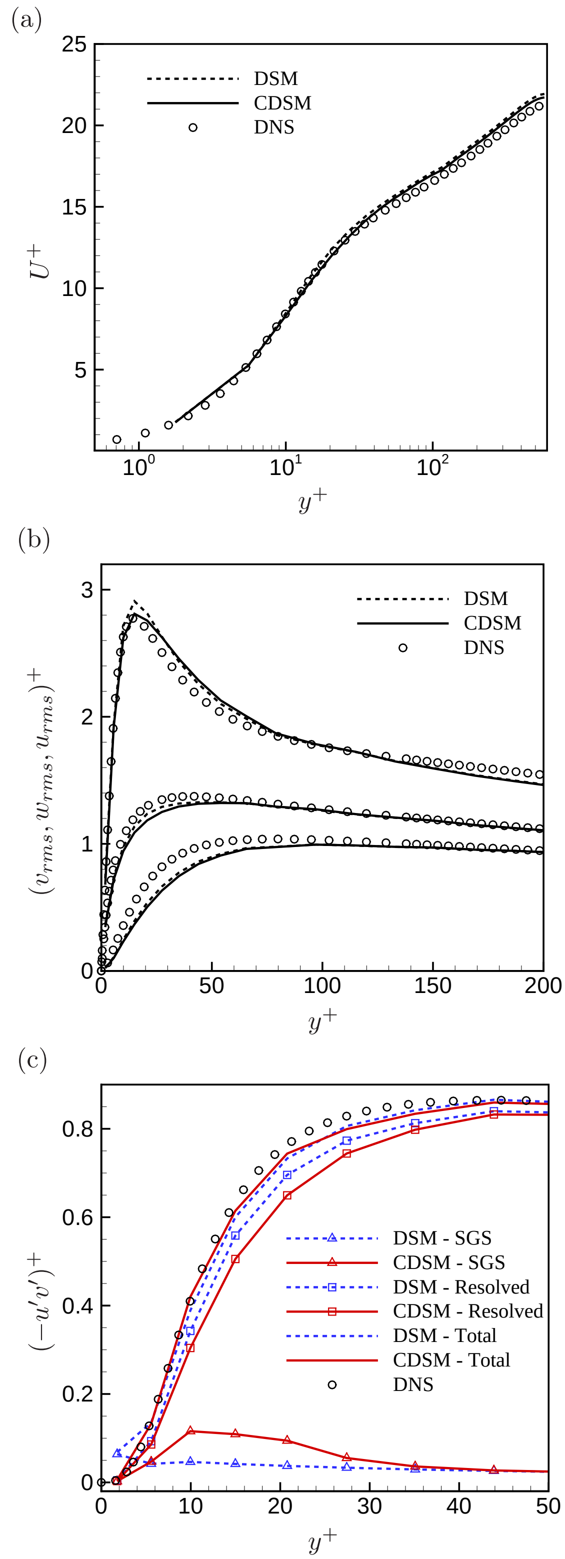

Figure 15: Mean statistics from turbulent channel flow at $Re_\tau = 590$ - Case 590un: (a) mean velocity, (b) rms velocity fluctuations, (c) Reynolds stress.

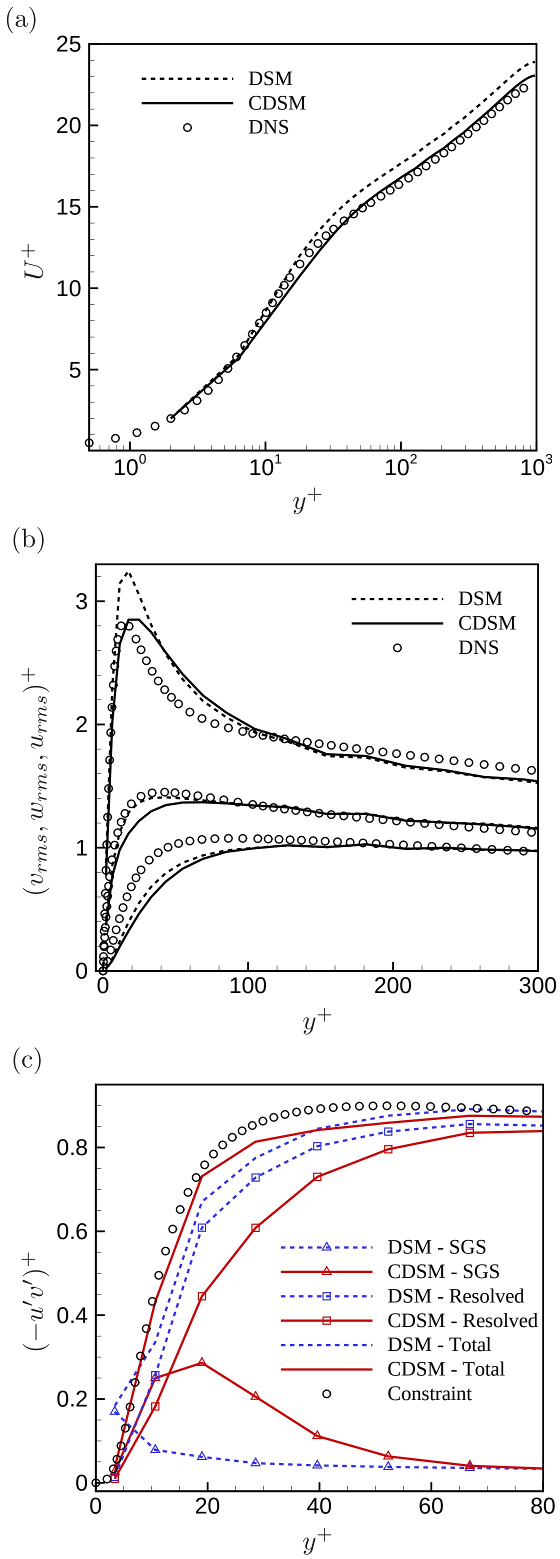

Figure 16: Mean statistics from turbulent channel flow at $Re_\tau = 1000$ - Case 1kun: (a) mean velocity, (b) rms velocity fluctuations, (c) Reynolds stress.

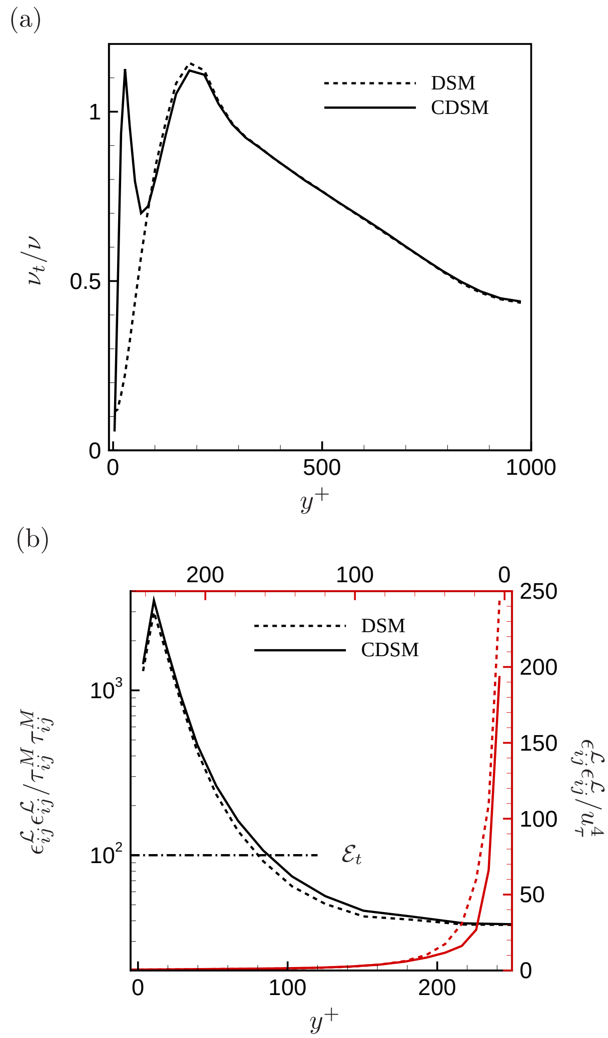

Figure 17: Mean statistics from turbulent channel flow at $Re_\tau = 1000$ - Case 1kun: (a) eddy-viscosity, (b) Germano-identity error.

CDSM. It also shows that only a few points near the wall have threshold $\mathcal{E}_t > 100$ (left side, black). Thus the constraint is active only at a few points near the wall ($y^+ < 100$).

At higher Reynolds numbers, the target Reynolds stress may not be easily available *a priori* from DNS, RANS or even experiments. A more convenient alternative is to use a model for Reynolds stress. Such models need only be reasonably accurate in the near-wall region as the constraint is only intended to be applied there. Results are shown at $Re_\tau = 1000, 2000$ with the Reynolds stress constraint obtained using the method described by Perry et al. (2002). Fig. 18 shows results at $Re_\tau = 2000$ from case 2kun with parameters $C_\omega = 0.1$, $\mathcal{E}_t = 100$. Note that the grid is almost the same as cases 590un and 1kun. This implies an even coarser

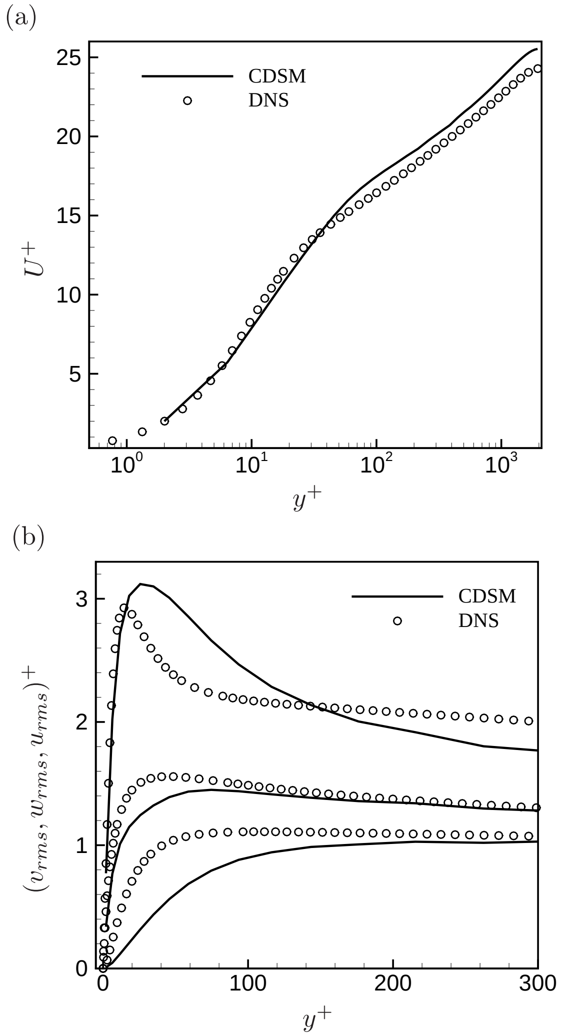

Figure 18: Mean statistics from turbulent channel flow at $Re_\tau = 2000$ - Case 2kun: (a) mean velocity, (b) rms velocity fluctuations.

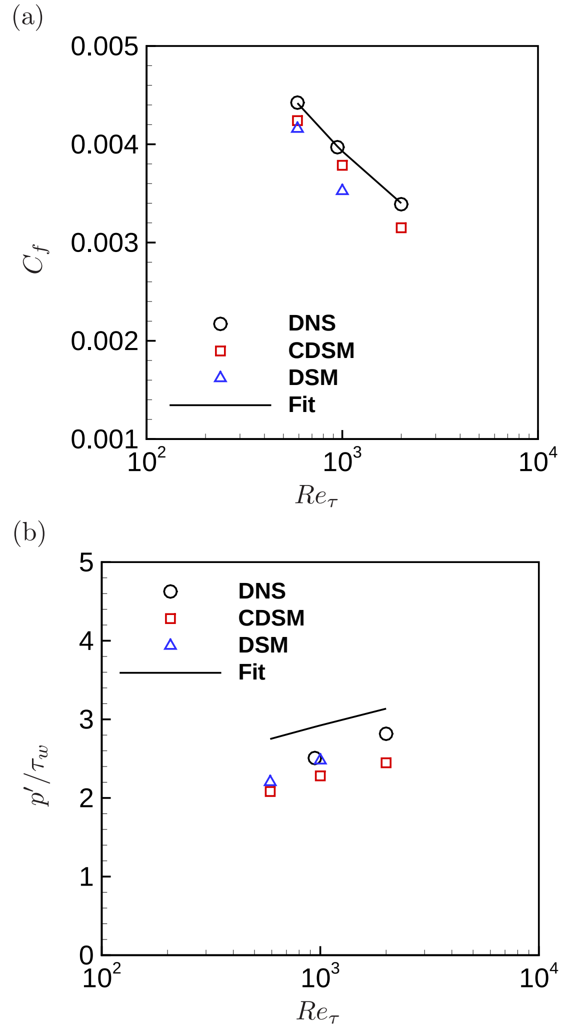

Figure 19: Comparison of (a) skin-friction coefficient C_f, and (b) wall pressure fluctuations $\sigma(p)/\tau_w$ from cases 590un, 1kun, 2kun.

Δz^+ and Δx^+ for this higher Reynolds number (as seen in table 4). The CDSM results for mean and rms u-velocity are in good agreement with unfiltered DNS. Though not shown here, DSM at such coarse resolution is expected to show significant differences with DNS.

Fig. 19 shows that skin-friction coefficient and wall pressure fluctuations obtained from CDSM are in reasonable agreement with the available DNS data and empirical fits. The skin-friction coefficient is based on the centerline velocity ($C_f = 2/U_{cl}^{+2}$). The fit shown is extrapolated from the DNS of Moser et al. (1999) by assuming $U_{cl}^+ = 21.26 + log(Re_\tau/587)/0.41$. This is done following Nikitin et al. (2000). Importantly, CDSM shows improvement over DSM. This improvement is expected to get very significant for LES at high Reynolds number on very coarse near-wall grids (such as for case 2kun). CDSM also predicts reasonable wall pressure fluctuations $\sigma(p)/\tau_w$ when compared to unfiltered DNS. The fit shown is taken from Bull (1996). It is encouraging that CDSM predicts unsteady behavior down to the wall along with quantities of engineering interest such as skin friction and wall pressure fluctuations.

CONCLUSION

This paper discusses two developments towards reliably using LES for attached high Reynolds number flows: (1) a dynamic Lagrangian model where a dynamic procedure is proposed for the Lagangian timescale and (2) a wall model where in addition to the Germano-identity error, external Reynolds stress is also imposed as a constraint on the ensemble-average subgrid-scale stress. Both developments are towards performing LES of complex flows on unstructured grids. They are in the context of the Dynamic Smagorinsky model (DSM) (Germano et al., 1991; Lilly, 1992) and exploit the Germano-identity error.

A dynamic Lagrangian averaging approach is developed for the dynamic subgrid scale model. The standard Lagrangian dynamic model (Meneveau et al., 1996) uses a Lagrangian time scale T_{LDSM} which contains an adjustable parameter θ. We propose to use a dynamic time scale T_{SC} based on a "surrogate-correlation" of the Germano-identity error (GIE) (Park and Mahesh, 2009). The proposed model is applied to LES of turbulent channel flow at moderately high Reynolds numbers and relatively coarse grid resolutions. Good agreement is obtained with unfiltered DNS data. Improvement is observed when compared to other averaging procedures for the dynamic Smagorinsky model, especially at coarse resolutions. The model is also applied to flow over a cylinder at a high Reynolds number. T_{SC} shows good agreement of turbulence statistics with previous computations and experiments, and is shown to outperform T_{LDSM}. It is established that T_{SC} is physically consistent with flow structures and hence a more apt choice for Lagrangian averaging. T_{SC} reduces the number of times adhoc clipping operations need to be performed on the computed eddy viscosity. Finally, the extra computational overhead incurred by the proposed Lagrangian averaging is negligible compared to when no averaging is used.

The strong scaling of the computing cost of LES with Reynolds number is an impediment to LES being applied to attached wall-bounded flows. However LES for wall-bounded flows offers the advantage of computing fluctuating quantities on the wall such as wall pressure fluctuations. A wall model (CDSM) is proposed to enable LES at coarse near-wall grid resolutions. The proposed model approaches the mean modeled behavior of RANS through a constraint on what is essentially an SGS model. Primarily, it allows hybridization of the LES methodology with a desired or expected mean target quantity; external Reynolds stress constraints are incorporated into the Dynamic Smagorinsky model. Secondly, this target quantity may be imposed in a small region near the wall for wall-bounded flows where SGS modeling errors are expected to be large; normalized Germano-identity error is used as a measure of SGS modeling errors and hence as a weight for the constraint. CDSM is applied to turbulent channel flows at various Reynolds numbers and grid resolutions. CDSM outperforms DSM and this improvement becomes more significant as the near-wall grid coarsens. CDSM achieves better predictions than DSM by constraining the total Reynolds stress to an *a priori* imposed target. It has been shown that this target Reynolds stress can be obtained from DNS and approximate near-wall models. Imposition of the Reynolds stress constraint in a small region near the wall increases the eddy viscosity and reduces the Germano-identity error near the wall. Importantly, this procedure does not force the instantaneous flow to a mean quantity but only constrains the mean behavior. Hence CDSM predicts unsteady behavior down to the wall and is a reliable tool to predict quantities of engineering interest such as skin friction and wall pressure fluctuations. For future work, CDSM will be applied to complex geometries and separated flows.

ACKNOWLEDGEMENT

This work was supported by the United States Office of Naval Research under ONR Grant N00014-05-1-0003 with Dr. Ki-Han Kim as technical monitor. Computing resources were provided by the Arctic Region Supercomputing Center of HPCMP and the Minnesota Supercomputing Institute.

References

Anderson, R. and Meneveau, C. "Effects of the similarity model in finite-difference LES of isotropic turbulence using a lagrangian dynamic mixed model". Flow, Turbulence and Combustion, 62:3: 201–225, 1999.

Baggett, J. S., Jiménez, J., and Kravchenko, A. G. "Resolution requirements in large-eddy simulations of shear flows". Annual Research Briefs, Center for Turbulence Research, Stanford Univ., 1997.

Bridges, D. H., Donnelly, M. J., and Park, T. J. "Experimental investigation of the submarine crashback maneuver". Journal of Fluids Engineering, 130, 2008.

Bull, M. K. "Wall-pressure fluctuations beneath turbulent boundary layers: some reflections on forty years of research". Journal of Sound and Vibration, 190:3:299–315, 1996.

Chang, P., Ebert, M., Young, Y. L., Liu, Z., Mahesh, K., Jang, H., and Shearer, M. "Propeller forces and structural responses to crashback". In Proceedings of the 27^{th} Symposium on Naval Hydrodynamics, Seoul, Korea, 2008.

Choi, J. I., Yeo, K., and Lee, C. "Lagrangian statistics in turbulent channel flow". Physics of Fluids, 16:779, 2004.

del Alamo, J. C., Jimenez, J., Zandonade, P., and Moser, Robert D. "Scaling of the energy spectra of turbulent channels". J. Fluid Mech., 500:135–144, 2004.

Franke, J. and Frank, W. "Large eddy simulation of the flow past a circular cylinder at $Re = 3900$". J. Wind. Eng. Ind. Aerodyn., 90:1191, 2002.

Germano, M., Piomelli, U., Moin, P., and Cabot, W. H. "A dynamic subgrid-scale eddy viscosity model". Physics of Fluids A, 3:7:1760, 1991.

Ghosal, S., Lund, T. S., Moin, P., and Akselvoll, K. "A dynamic localization model for large-eddy simulation of turbulent flows". J. Fluid Mech, 286: 229, 1995.

Hoyas, S. and Jimenez, J. "Scaling of the velocity fluctuations in turbulent channel flow up to $Re_\tau = 2003$". Physics of Fluids, 18:011702, 2006.

Inagaki, M., Kondoh, T., and Nagano, Y. "A mixed-time-scale SGS model with fixed model-parameters for practical LES". Engineering Turbulence Modeling and Experiments 5, pages 257–266, 2002.

Jang, H. Large eddy simulation of Crashback in marine propulsors. PhD thesis, University of Minnesota, 2011.

Jang, H. and Mahesh, K. "Large eddy simulation of marine propellers in crashback". In Proceedings of the 28^{th} Symposium on Naval Hydrodynamics, Pasadena, CA, 2010.

Jang, H. and Mahesh, K. "Large eddy simulation of flow around a reverse rotating propeller". In review, Journal of Fluid Mechanics, 2012.

Kravchenko, A. G. and Moin, P. "Numerical studies over a circular cylinder at $Re_D = 3900$". Physics of Fluids, 12:2:403–417, 2000.

Lilly, D. K. "A proposed modification of the germano subgrid–scale closure model". Physics of Fluids A, 4:3:633, 1992.

Mahesh, K., Constantinescu, G., and Moin, P. "A numerical method for large–eddy simulation in complex geometries". Journal of Computational Physics, 197:1:215, 2004.

Meneveau, C. and Lund, T. S. "On the lagrangian nature of the turbulence energy cascade". Physics of Fluids, 6:2820, 1994.

Meneveau, C., Lund, T. S., and Cabot, W. H. "A lagrangian dynamic subgrid-scale model of turbulence". J. Fluid Mech., 319:353, 1996.

Moser, R. D., Kim, J., and Mansour, N. N. "Direct numerical simulation of turbulent channel flow up to $Re_\tau = 590$". Physics of Fluids, 11:943, 1999.

Nicoud, F., Baggett, J. S., Moin, P., and Cabot, W. "Large eddy simulation wall-modeling based on suboptimal control theory and linear stochastic estimation". Physics of Fluids, 13:2970, 2001.

Nikitin, N.V., Nicoud, F., Wasistho, B., Squires, K.D., and Spalart, P.R. "An approach to wall modeling in large-eddy simulations". Physics of Fluids, 12:1629, 2000.

Park, N. and Mahesh, K. "A velocity-estimation subgrid model constrained by subgrid scale dissipation". J. Comput. Phys., 227:4190, 2008a.

Park, N. and Mahesh, K. "A dynamic wall model constrained by external reynolds stress". In Proceedings of XXII ICTAM, Adelaide, Australia, 2008b.

Park, N. and Mahesh, K. "Reduction of the germano identity error in the dynamic subgrid model". Physics of Fluids, 21:065106, 2009.

Perry, A. E., Marusic, I., and Jones, M. B. "On the streamwise evolution of turbulent boundary layers in arbitrary pressure gradients". J. Fluid Mech., 461:61–91, 2002.

Piomelli, U. "Wall-layer models for large-eddy simulations". Progress in Aerospace Sciences, 44:437–446, 2008.

Piomelli, U. and Balaras, E. "Wall-layer models for large-eddy simulations". Annual Review Fluid Mechanics, 34:349–74, 2002.

Piomelli, U., Yu, Y., and Adrian, R. J. "Subgrid-scale energy transfer and near-wall turbulence structure". Physics of Fluids, 8:1978, 1996.

Rovelstad, A. L., Handler, R. A., and Bernard, P. S. "The effect of interpolation errors on the lagrangian analysis of simulated turbulent channel flow". Journal of Computational Physics, 110:1: 190–195, 1994.

Sarghini, F., Piomelli, U., and Balaras, E. "Scale-similar models for large-eddy simulations". Physics of Fluids, 11:6:1596–1607, 1999.

Shi, Y., Xiao, Z., and Chen, S. "Constrained subgrid-scale stress model for large eddy simulation". Physics of Fluids, 20:011701, 2008.

Smagorinsky, J. "General circulation experiments with the primitive equations: I. The basic experiment". Mon. Weath. Rev., 91:99, 1963.

Spalart, P.R., Jou, W.H., Strelets, M., and Allmaras, S.R. "Comments on the feasibility of LES for wings and on a hybrid RANS/LES approach". In First AFOSR International Conference on DNS/LES, Ruston, Louisiana. Greyden Press, 1997.

Stoll, R. and Porté-Agel, F. "Dynamic subgrid-scale models for momentum and scalar fluxes in large-eddy simulations of neutrally stratified atmospheric boundary layers over heterogeneous terrain". Water Resources Research, 42:W01409, 2006.

Stoll, R. and Porté-Agel, F. "Large-eddy simulation of the stable atmospheric boundary layer using dynamic models with different averaging schemes". Boundary-Layer Meteorology, 126:1–28, 2008.

Templeton, J. A., Medic, G., and Kalizin, G. "An eddy-viscosity based near-wall treatment for coarse grid large-eddy simulation". Physics of Fluids, 17:105101, 2005.

Templeton, J. A., Wang, M., and Moin, P. "An efficient wall model for large-eddy simulation based on optimal control theory". Physics of Fluids, 18: 025101, 2006.

Tremblay, F., Manhart, M., and Friedrich, R. "DNS of flow around a circular cylinder at a subcritical reynolds number with cartesian grids". In Proceedings of the Eighth European Turbulence Conference, Barcelona, Spain, EUROMECH, CIMNE, pages 659–662, 2000.

Vasilyev, O. V., Stefano, G. De, Goldstein, D. E., and Kevlahan, N. K.-R. "Lagrangian dynamic SGS model for stochastic coherent adaptive large eddy simulation". Journal of Turbulence, 9, 2008.

Verma, A., Jang, H., and Mahesh, K. "Large eddy simulation of the effect of hull on marine propulsors in crashback". In Proceedings of the 2^{nd} International Symposium on Marine Propulsors, Hamburg, Germany, 2011.

Verma, A., Jang, H., and Mahesh, K. "The effect of upstream hull on a propeller in reverse rotation". In review, Journal of Fluid Mechanics, 2012.

Vyšohlid, M. and Mahesh, K. "Large eddy simulation of propeller crashback". In Proceedings of Flow Induced Unsteady Loads and the Impact on Military Applications, RTO-MP-AVT-123, Neuilly-sur-Seine, France, 2005.

Vyšohlid, M. and Mahesh, K. "Large eddy simulation of crashback in marine propellers". In Proceedings of the 26^{th} Symposium on Naval Hydrodynamics, Rome, Italy, 2006.

You, D., Wang, M., and Mittal, R. "A methodology for high performance computation of fully inhomogeneous turbulent flows". Int. J. for Numerical Methods in Fluids, 53:6:947–968, 2007.